The Mass/Light Ratio of Early-Type Galaxies: Constraints from Gravitational Lensing in the Rich Cluster AC114*

Priyamvada Natarajan[1], Jean-Paul Kneib[2], Ian Smail[3] & Richard S. Ellis[1]

1) Institute of Astronomy, Madingley Road, Cambridge, CB3 0HA, UK

2) Observatoire Midi-Pyrenees, 14 Av. E. Belin, 31400 Toulouse, France

3) Department of Physics, University of Durham, South Rd Durham, UK

Received —; accepted —

*Based on observations with the NASA/ESA *Hubble Space Telescope* obtained at the Space Telescope Science Institute, which is operated by the Association of Universities for Research in stronomy Inc., under NASA contract NAS 5-26555.

ABSTRACT

We present a new wide field image of the distant cluster AC114 ($z = 0.31$) obtained with *Wide Field and Planetary Camera II* onboard the *Hubble Space Telescope*. This image considerably extends our knowledge of the lensing properties of the cluster beyond that derived by Smail et al. (1995a) from a single WF/PC-1 pointing. In conjunction with published ground-based spectroscopy, we utilise several newly-discovered multiple images to construct an improved mass model for the central regions of the cluster. Using this model, we apply the methodology introduced by Natarajan & Kneib (1997) to interpret local perturbations to the cluster shear field on small scales resulting from mass associated with individual cluster galaxies. We use the lensing signal to place new constraints on the average mass-to-light ratio and spatial extents of the dark matter halos associated with morphologically-classified early-type cluster members. We find that the total mass of a fiducial L^* cluster spheroidal galaxy is largely contained within ~ 15 kpc radius halo ($\sim$ 8–10 R_e) with a mass-to-light ratio $M/L_V \sim 15^{+10}_{-4}$ (90 % c.l.) in solar units within this radius. Comparisons with similar estimates for field galaxies suggests that the cluster galaxies in AC114 may possess less extensive and less massive halos. Additionally, we find some indication that, at a fixed luminosity, S0 galaxies are less extended than ellipticals, suggesting a difference in the efficiency of tidal stripping of different galaxy types. We discuss the consequences of our results in the context of models for the dynamical evolution of cluster galaxies and the observational prospects for extending such analyses.

Subject headings: cosmology: observations – cosmology: gravitational lensing

1. Introduction

The distortions induced in the shapes of faint background galaxies by the gravitational lensing of a foreground cluster offers a powerful way of reconstructing the mass distribution of the intervening lens (Mellier et al. 1997). While weak lensing studies have addressed the distribution of mass on large scales ($\gtrsim$ 300 kpc†, Smail et al. 1995b; Squires et al. 1996), analysis of strongly lensed features has allowed more detailed modelling of the morphology of the total mass on small scales ($\gtrsim$ 20 kpc) in the central regions of a few clusters, e.g. Cl0024+16 (Kassiola, Kovner & Fort 1993) and A2218 (Kneib et al. 1996). These latter studies have suggested that mass concentrations associated with individual cluster galaxies are needed to fit the detailed geometry of some giant arcs.

This paper is concerned with examining the role of galaxy halos in defining the distribution of mass in clusters on intermediate scales ($\simeq$ 50 kpc) across a range of environments within clusters from the core regions to the lower density outskirts. Our technique considers perturbations associated with an ensemble of cluster galaxies within a smooth global cluster potential. Such perturbations can be derived from the shape of the gravitational shear field estimated via the distorted forms of faint background galaxies. A strong motivation for this work is the need to examine whether the mass-to-light ratio (M/L) of galaxies (measured within a large effective aperture) varies significantly between high density cluster regions and the field. Such an environmental variation of the M/L ratio of a galaxy might be expected if these galaxies presently found in dense regions suffered more complex interaction histories leading to a redistribution of the associated gaseous, stellar and dark matter components (c.f. Moore et al. 1996). One possibility is that the extended dark halo would be preferentially removed and redistributed, leading to a reduction in the M/L ratio compared to that found for isolated galaxies of the same morphological type. However, the scale on which this redistribution occurs (and hence the 'granularity' of the resultant dark matter distribution within the cluster) is unclear and has important implications for our understanding of how clusters assemble and evolve.

Previous estimates of the global M/L of galaxies on intermediate scales relate primarily to field galaxies and have been obtained from dynamical studies of their satellite systems (Zaritsky et al. 1993), the rotational motion of the HI gas (Sackett 1995), as well as the kinematics of the stellar component (Rix et al. 1997). Recently weak lensing analyses have been applied to provide constraints on the mass distributions on intermediate-large scales around ensembles of field galaxies (Brainerd, Blandford & Smail

†Throughout the analysis we have assumed $\Omega = 1$; $\Lambda = 0$; $H_0 = 50$ km/s/Mpc which corresponds to an angular scale of $1'' = 5.605$ kpc at $z = 0.31$.

1996, hereafter BBS), a similar approach to that used here. Their statistical analysis of the alignment of the faint field population around bright foreground galaxies gives a characteristic lensing mass of $M = (2.0^{+2.4}_{-1.0}) \times 10^{12} M_{\odot}$ (90% c.l.) within a radius of 200 kpc (at a median galaxy redshift of $z \sim 0.5$). This corresponds to a $M/L_V = 100^{+110}_{-60}$ in solar units within their large aperture. Their analysis also provided weak limits on the scale of the halo around these galaxies, a typical extent less than 20 kpc was rejected at the 2 σ level, while the upper limit on the halo size was unconstrained, $r_t \gtrsim 200$ kpc. Modelling field galaxies as truncated isothermal spheres, Dell'Antonio & Tyson (1996; DT hereafter) have obtained modest limits on the central velocity dispersion and outer radius via a galaxy-galaxy lensing analysis of the Hubble Deep Field. Using a very small aperture they find a central velocity dispersion $\sigma = 185^{+30}_{-35}$ km s^{-1}, $r_{\rm outer} \geq 30$ kpc, and an average mass enclosed within 20 kpc of $(1.2^{-5.4}_{+5.0}) \times 10^{12} M_{\odot}$.

In this paper we examine whether it is observationally feasible to detect the granularity in the cluster mass distribution and hence place limits on the sizes and masses of dark matter halos associated with typical galaxies **within** a rich cluster. To do this we analyse a new wide-field *Hubble Space Telescope* (*HST*) image of the rich cluster AC114 ($z = 0.31$) in §2. We construct a detailed model of the large-scale mass distribution within the cluster using the numerous strongly-lensed features visible in the *HST* data in §3. The new image allows us to improve upon the earlier model presented by Smail et al. (1995a) on the basis of pre-refurbishment *HST* data. Of considerable importance is the simplicity of our overall mass distribution in the central regions; only a single, regular mass concentration is visible both in the lensing shear field or the cluster X-ray emission (Smail et al. 1995a), making AC114 an ideal cluster for our purposes.

We use techniques developed in the theoretical discussion given by Natarajan & Kneib (1995, 1997; hereafter NK) and examining the weakly lensed arclets seen through the cluster we search for local perturbations in the cluster potential and correlate these with cluster galaxies of known morphology and luminosity. In this way we provide new constraints on the M/L and extent of their dark halos. Section 4 describes the formalism used to place limits on the mass associated with individual cluster galaxies, while §5 presents our results and §6 discusses these and gives our main conclusions.

2. Data

The rich cluster AC114 (z=0.31) was observed with the *WFPC2* during Cycle 5 for a total of 24 orbits through the F702W filter. The observations were mosaiced across four different pointings each of 16.8 ks total integration to give a contiguous field of $\sim 6.5' \times 3.9'$ (c.f. Fig. 1). In addition, by positioning one of the WFC chips on exactly the same region in two of the pointings, a deeper exposure (33.6 ks) was achieved for a $80'' \times 80''$ field in the cluster center. The six orbits at each pointing were split into 3 pairs, each of

which was spatially offset by 3 WFC pixels to enable the removal of hot pixels and similar artefacts.

The data was reduced using the standard STScI pipeline followed by alignment with integer pixel shifts and stacking based on the the STSDAS task CCREJ. Cataloging and photometry of objects on these coadded frames was accomplished using the Sextractor image analysis package (Bertin & Arnouts 1996). Image detection proceeded by first convolving the data with a 0.3 arcsec diameter box filter and applying a surface brightness threshold of $\mu_{702} = 25.0$ mag arcsec^{-2} (corresponding to 1.3σ of the sky noise) and a minimum object area of 12 contiguous pixels. The Sextractor package provides 'Kron' magnitudes for each object which we have placed on the R_{702} system using zero-points published by Holtzman et al. (1995).

Unfortunately, due to an error in the scheduling of the observations, the *HST* images have ~ 4–$5\times$ the nominal sky background, restricting the limiting magnitude at which reliable image shapes can be determined to $R_{702} = 26$ rather than the expected $R_{702} \sim 26.5$–27 (the *WFPC2* observations of the central field will be repeated in Director's discretionary time in the near future). Although the surface density of useable background images overall is considerably reduced, the gain over the earlier WF/PC-1 data is still substantial, particularly in the double pointing of the center region.

We show in Fig. 1 the central area of the *HST* field, as in A2218 (Kneib et al. 1996) the high resolution imaging provided by *HST* uncovers a wide range of strongly lensed features in the center of the cluster lens. In Fig. 2 we provide more detailed views of these features to highlight their lensed nature. The most prominent feature, originally discovered by Smail et al. (1995a) as S1/S2, is the hook-shaped $z = 1.86$ galaxy for which we can now locate the missing third image S3 (Fig. 2). The geometrical configuration of these three images, together with the spectroscopic redshift, provides a reliable absolute calibration of the mass in the central regions of the cluster (see §3). Based on this calibration and assuming the general morphology of the cluster potential as indicated by the X-ray map (Smail et al. 1995a), we can derive estimates of the likely redshifts of the other multiply-imaged sources in the field. A major breakthrough provided by the new *HST* image is the identification of three 5-fold multiply-imaged systems A1–5 (with a predicted redshift of $z = 1.67 \pm 0.15$ from our lens model), B1–5 ($z = 1.17 \pm 0.10$) and D1–5 ($z = 1.18 \pm 0.10$).[‡] The former includes a radial feature (A4–A5) which provides an important constraint on the inner-most regions of the cluster potential. B1–5 represents a three-image 'cusp' configuration perturbed by a nearby cluster elliptical, adding two more images (B3–B4). D1–5 is a cusp arc (3 images) perturbed by the two big ellipticals near the cD galaxy. Each perturbing galaxy adds 2 images to the system, but only one is visible, as the other one

[‡]As some of these images were previously unmatched with their counterparts, it is convenient to introduce a new nomenclature. We note that B2=A1; C2=A2; C1=A4; A2=A5; B3=A6 where we give our nomenclature first and then Smail et al.'s.

is de-amplified and lies at the center of each galaxy. Arguably the most startling multiply-imaged feature in the cluster is C1-3, three images of a partial-ring shaped galaxy which we estimate to lie at $z = 2.1 \pm 0.3$. The highly elongated morphology of the source, with several bright knots lying along the ridge, provides an unique insight into the morphological nature of galaxy formation at high redshift. A number of other fainter candidate multiple images are visible around the cD. We postpone detailed discussion of these features until the deeper pointing of this field has been acquired. We demonstrate below that the lensed features catalogued here (Fig. 1, 2) are sufficient to allow us to both improve the mass model over the earlier one developed by Smail et al. (1995a) and to search for the granularity due to individual cluster galaxies on a statistical basis.

The image catalog constructed from our frames contains 2446 objects brighter than $R_{702} = 26$ over the 25 sq. arcmin of the field. We have adopted a bright magnitude cut-off of $R_{702} = 23$ for our background field sample in order to reduce contamination by foreground and cluster galaxies. Within $23 < R_{702} < 26$, all 1762 galaxies were therefore considered as background. The R_{702} magnitudes were converted into the rest-frame V-band assuming a non-evolving E/S0 spectral energy distribution to determine the k-correction. To select perturbing galaxies within the cluster we made use of the morphologically-classified catalogue of Couch et al. (1997). To study the morphological mix within the cluster these workers determined visual classifications for 485 galaxies brighter than $R_{702} = 23.0$ ($M_V = -16.3$, assuming a non-evolving elliptical spectral energy distribution) in the field of AC114. A subset of 208 were classified as spheroidal (E or S0). In detail, the morphological breakdown to R_{702}=23.0 is as follows: E (52), E/S0 (69) and S0+S0/a (87) (Couch et al. 1997). The median luminosity for the sample limited at this apparent magnitude is close to the characteristic luminosity L^* of the cluster population. To a limit of $R_{702} = 21.0$ the equivalent numbers are: E (22), E/S0 (10) and S0+S0/a (44). The central cD was removed from further consideration since its halo is expected to differ significantly from that of the average cluster member.

3. Cluster Mass Modelling

Considerable progress has been made in the interpretation of the observed shear field in clusters, using the inversion technique first described by Kaiser & Squires (1993), a refined version developed by Seitz & Schneider (1995) as well as through local finite field inversion techniques suggested by Kaiser (1995) and Schneider (1995). These methods are appropriate for low resolution mapping in the weak regime. Better resolution is possible in the central regions of the cluster where strong lensing effects are prominent. Our approach following NK (described below) extends both the χ^2 model fitting of Kneib et al. (1996) as well as building upon the techniques of BBS and their maximum likelihood extension (Schneider & Rix 1997).

Both strong and weak lensing constraints are included in this mass reconstruction procedure for clusters as traced by the observed shear field.

An accurate mass model for AC114 is an essential prerequisite to the various galaxy-galaxy lensing methods discussed in §4. The large number of multiply-imaged features identified from the new *WFPC2* imaging of AC114 means that an accurate model is feasible, especially when these multiply-imaged features are combined with the observed radial profile of the smoothed tangential shear. Here we follow closely the methodology of Kneib et al. (1996), constraining the morphology of the cluster mass distribution with the positions and relative amplifications of the 5 sets of multiple images (above) as well as the large-scale weak shear field. The iso-density contours are shown in Fig. 1. The simplicity of the cluster mass distribution as indicated by both the lensing shear field and the cluster X-ray emission (Smail et al. 1995a), make AC114 an ideal cluster for our purposes. Further detailed comparison of our lensing model with numerical cluster simulations (including the hydro-dynamics of the gas) as well as the X-ray data will be dealt with in a forthcoming paper. Our best-fit model for the central regions ($r \leq 250$ kpc) has a single, dominant potential centered on the cD, with an ellipticity and orientation close to that of the cD halo (Table 1). The total masses within 75; 150; 500 kpc of the cluster centre are respectively $(0.42 \pm 0.01) \times 10^{14} M_{\odot}$; $(1.2 \pm 0.15) \times 10^{14} M_{\odot}$ and $(4.0 \pm 0.4) \times 10^{14} M_{\odot}$. The total mass-to-light ratio for AC114 out to 500 kpc is found to be $M/L_V \sim 160 (M/L_V)_{\odot}$.

4. Galaxy-Galaxy Lensing Methods

4.1. Formalism

The cluster potential ($\phi_{\rm tot}$) in AC114 is treated as a linear superposition of a smooth large-scale potential ($\phi_{\rm c}$) with a typical scale > 20 arcsec and several small-scale perturbations ($\phi_{\rm cgal_i}$) representing cluster galaxies and their associated halos, i.e.

$$\phi_{\rm tot} = \phi_{\rm c} + \Sigma_i \, \phi_{\rm cgal_i}, \tag{1}$$

As shown by NK, the complex shear g evaluated for such a potential in the frame of the perturber can be written as a sum of contributions arising from the intrinsic shapes of the sources, that induced by the smooth cluster component and that from the small-scale perturbers (see §2.2 of NK for details). The small-scale potentials are represented by pseudo-isothermal elliptical mass distributions (Kassiola & Kovner 1993) and each is characterised by a central velocity dispersion (σ_0), a core-radius (r_0) set to be 0.15 kpc for a L^* galaxy and a truncation radius (r_t). To minimize the number of parameters needed to characterize a fiducial galaxy, a set of scaling laws physically motivated by the Fundamental Plane (FP), similar to those

used by BBS are adopted:

$$\sigma_0 \,=\, \sigma_{0*}(\frac{L}{L^*})^{\frac{1}{4}};\;\; r_0 \,=\, r_{0*}(\frac{L}{L^*})^{\frac{1}{2}};\;\; r_t \,=\, r_{t*}(\frac{L}{L^*})^{\alpha}. \tag{2}$$

The total mass, M, and the mass-to-light ratio, Υ, scale as:

$$M \,=\, 2\pi\Sigma_0 r_0 r_t \,=\, \frac{9}{2G}{\sigma_{0*}}^2 r_{t*}(\frac{L}{L^*})^{\frac{1}{2}+\alpha}\,; \tag{3}$$

$$\Upsilon \,= 21\,\left(\frac{\sigma_{0*}}{240\,\mathrm{km\,s^{-1}}}\right)^2\left(\frac{r_{t*}}{15\,\mathrm{kpc}}\right)\left(\frac{L}{L^*}\right)^{\alpha-\frac{1}{2}}, \tag{4}$$

where Σ_0 represents the projected mass density at the lens and α is an index that is assigned a value of 0.5 yielding the constant mass-to-light ratio case or a value of 0.8 leading to $\Upsilon \,\sim\, L^{0.3}$ consistent with the observed correlations on the FP (e.g. Jorgensen et al. 1996).

4.2. Direct Aperture Averaging Method

The simplest approach toward measuring the granularity in the shear pattern is to average the mean gravitational shear within apertures around each of the cluster galaxies. This 'direct' method does not require an accurate description of the smooth cluster mass distribution and consequently yields only approximate limits on the mean M/L ratio on intermediate scales. Nevertheless, in the weak regime, the large scale shear contribution will vary at most linearly across a given annulus, making subtraction straightforward. The residual tangential component of the shear in the frame of an individual perturbing galaxy then constrains the typical galaxy M/L through the various scaling relationships given in §3.1. The signal to noise of these measurements depends not only upon the masses of the galaxies, but also on a number of other factors of which the surface density of background sources is the most important (NK).

4.3. Maximum Likelihood Method

While the direct averaging method is straightforward to apply, to robustly and independently constrain both of the fiducial parameters of interest (σ_{0*} and r_t) the large-scale mass distribution needs to be taken into account in the non-linear, over-critical central regions of the cluster. The maximum likelihood method proposed in NK allows us to do this and we now describe its application to our observations of AC114. The essential procedure is to maximize the likelihood function of the predicted distribution for the ellipticities of the background sources, using a set of model parameters for the cluster galaxies, given the distributions of intrinsic ellipticity and redshift for the faint field population. In the weak regime, the intrinsic ellipticity

vector τ_{S_j} of the jth faint background galaxy can be determined from its observed ellipticity vector $\tau_{\rm obs_j}$ by subtracting the induced shear vector from the various components of the cluster lens:

$$\tau_{S_j} \; = \; \tau_{\rm obs_j} \; - \Sigma_i^{N_{\rm cgal}} \, \gamma_{{\rm cgal}_i} \; - \; \gamma_{\rm c}, \tag{5}$$

where $\Sigma_i^{N_{\rm cgal}} \, \gamma_{{\rm cgal}_i}$ is the sum of the shear contribution at a given position j from $N_{\rm cgal}$ perturbers, and the term $\gamma_{\rm c}$ is the shear induced by the smooth cluster component. Note here that the expression in eqn. (5) above is the form obtained in the limiting case of the weak regime - where the effects of magnification are small, for the maximum likelihood analysis, we use the full non-linear relation to incorporate both the strong and weak lensing regimes as described in NK. For each arclet, a redshift is assigned from the expected redshift distribution $N(z)$ corresponding to its intrinsic magnitude. Limits on the $N(z)$ at such faint limits can be provided by classical spectroscopy (Cowie et al. 1996), with alternative estimates provided through inversion techniques employing highly-constrained cluster lenses (Kneib et al. 1996, 1997), and photometric modelling of the Hubble Deep Field (e.g. Metcalfe et al. 1996; Mobasher et al. 1996; Lanzetta et al. 1996; Connolly et al. 1997). We adopt the $N(z)$ derived for an $R_{702} \sim 25$ distribution by Kneib et al. (1996) extrapolating it slightly using the no evolution predictions when necessary. For moderate redshift cluster lenses the uncertainties associated with the redshift distribution of background galaxies are no longer a major concern (Ellis 1997). The intrinsic shape for the background source is also randomly assigned from the distribution measured in blank fields imaged with *WFPC2* using the Medium Deep Survey data and other similar *HST* archival *WFPC2* data (Ebbels et al. 1998).

Given a detailed mass model for the cluster, $\gamma_{\rm c}$ can be specified so the likelihood for a proposed self-similar parameter set for the cluster galaxies (eqn. 2) can be expressed as:

$$\mathcal{L}(\sigma_{0*}, r_{t*}) = \Pi_j^{N_{bgal}} p(\tau_{S_j}). \tag{6}$$

The likelihood function of the estimated probability distribution of the source ellipticities (given that the functional form of the intrinsic ellipticity distribution is assumed to be known for field galaxies from the MDS) is maximized with respect to the model parameters (σ_{0*}, r_{t*}) and is optimized for agreement with the constraints from the strong lensing (the sets of multiple images) in the central regions.

In principle, the likelihood function $\mathcal{L}$ needs to be computed for many different realizations, i.e. the redshift drawn for any individual image in fact needs to be the mean over different draws. However, we demonstrate below that it is equivalent to constructing the likelihood for a single realization where the redshift z_j of the arclet drawn is the median redshift corresponding to the observed source magnitude from $N(z, m_j)$. On performing a Monte-Carlo sum over $N_{\rm MC}$ realizations of z_j, the likelihood becomes:

$$\mathcal{L}(\sigma_{0*}, r_{t*}, ...) = \Pi_j^{N_{gal}} \Pi_k^{N_{\rm MC}} p(\tau_{S_j^k}), \tag{7}$$

where $p_\tau(\tau_{S_j^k})$ is the probability of the source ellipticity distribution at the position j for k drawings for the redshift of an arclet of magnitude m_j. The mean over $N_{\rm MC}$ realizations gives:

$$\big\langle p(\tau_{S_j})\big\rangle \;=\; \frac{1}{N_{\rm MC}}\,\Sigma_{k=1}^{N_{\rm MC}}\,p(\tau_{S_j^k}). \tag{8}$$

It is equivalent to the following expression in integral form,

$$\begin{aligned}\big\langle p(\tau_{S_j})\big\rangle \;&=\; \frac{\int p(\tau_{S_j}(z))N(z,m_j)\,dz}{\int N(z,m_j)\,dz} \\ &=\; p(\tau_{S_j}(z_{\rm avg}))\;\sim\; p(\tau_{S_j}(z_{\rm median}))\end{aligned} \tag{9}$$

$z_{\rm avg}$ being the average redshift corresponding to the magnitude m_j. We define $z_{\rm avg}$ so that $p(\tau_{S_j}(z_{\rm avg}))$ is equal to $\big\langle p(\tau_{S_j})\big\rangle$, and since both the ellipticity distribution and the redshift distribution are 'broad' $z_{\rm avg}$ is nearly equal to $z_{\rm median}$ - the median redshift of the magnitude limited arclet sample. Therefore the corresponding likelihood $\mathcal{L}$ can then be simply written as,

$$\mathcal{L} \;=\; \Pi_j\big\langle p(\tau_{S_j})\big\rangle \tag{10}$$

and the log-likelihood as $l \;=\; \ln\mathcal{L} \;=\; \Sigma\big\langle p(\tau_{S_j})\big\rangle$. The best estimate of the model parameters are obtained by maximizing this log-likelihood function with respect to σ_{0*} and r_{t*}. Geiger & Schneider (1997) have also recently demonstrated the robustness of such a maximum-likelihood implementation.

From the simulations presented in Section 5.4 of NK, it was found that for robust results the cluster model used to derive $\gamma_{\rm c}$ (based upon strongly-lensed features) must have a centre known to $\pm$ 5 arcsec and an Einstein radius to within 20%. Our model of AC114 discussed in §3 attains the necessary accuracy (c.f. Table 1).

5. Results

We first present the results from our direct estimation of galaxy-galaxy lensing in AC114. Direct averaging of the shear field on small scales around the 208 E and S0 cluster galaxies defined as perturbers in our analysis does provide a weak detection. The signal is computed in annuli centred around the perturbing galaxies. The strongest signal as expected lies within the innermost bin, corresponding to a radius of less than 1.5 arcsec. The measured value of the shear there is $\tau \;=\; 0.16^{+0.12}_{-0.13}$ (1σ). Simulating the composite mass distribution in AC114 (i.e. including the cluster members and the model described in § 3), using the methodology described in § 4 of NK, this measured value of τ is translated into a M/L_V. For a L^* galaxy the physical radius that corresponds to the outer-most annulus is $\sim$ 35 kpc. Subdividing the sample of cluster galaxies into morphological classes, we find that the signal is dominated by the brighter, spheroidal

galaxies for which we find $M/L_V \sim 16^{+8}_{-12}(M/L_V)_\odot$ within 35 kpc. These errors have been assigned on the basis of simulations of the constructed composite mass model (main clump + cluster galaxies), and therefore include the effects of the assumed linearity of the potential induced by this smooth clump on large scales.

Turning to our maximum likelihood analysis, we also report a signal detection (Figs 3). These figures show that we can set joint constraints on both the central masses of the cluster galaxies and their halo sizes. In Fig. 3a, we utilised the entire sample of cluster galaxies adopting $\alpha = 0.5$ which yields a well-defined likelihood peak at $\sigma_0^* = 192^{+53}_{-27}$ km s^{-1} ($\sigma_0^* > 250$ km s^{-1} is excluded at 95% c.l.) and $r_t \approx 17$ kpc. These values translate into a total mass for an L^* galaxy of $M \sim (4.9^{+3.1}_{-1.3}) \times 10^{11}\, M_\odot$ and an average $M/L_V \sim 15^{+10}_{-4}(M/L)_\odot$. Note that only the dispersion in the value of σ_0 is used in the computation of the 90% c.l. error bars quoted above.

In Fig. 3b, we illustrate the effect of adopting $\alpha = 0.8$. In this case, the likelihood has a maximum at $\sigma_0^* = 208^{+17}_{-12}$ km s^{-1} ($\sigma_0^* > 250$ km s^{-1} once again excluded at 95% c.l.) and $r_t \approx 18$ kpc. These values translate into a typical total mass for an L^* galaxy of $M \sim (6.1^{-0.7}_{+1.1}) \times 10^{11}\, M_\odot$ or an average $M/L_V \sim 19^{+4}_{-2}$ in solar units.

Taking $\alpha = 0.5$ and fixing the fiducial halo size obtained above ($r_t = 17$ kpc), we finally split the sample into E's and S0's and compute the likelihood estimate for their characteristic velocity dispersions at a fixed luminosity independently. We note here that the median luminosities and ranges for the two categories are very similar. We find a marginal indication that the E galaxies are more massive than the S0s within our effective radius: $\sigma_0(E) = 190^{+15}_{-52}$ km s^{-1} and $\sigma_0(S0) = 120^{+17}_{-32}$ km s^{-1} (Fig. 3c). At the 60 % c.l., E's and S0's seem to have differing characteristic central velocity dispersions, which can be attributed to arising from structural differences, for instance, due to differences in their truncation radii.

The reliability of these conclusions has been tested via extensive simulations and tests. In particular we have conducted several null tests by randomising (i) the orientation of the background sources, (ii) the positions of the background sources within the frame, and (iii) the lens centers. In each case no significant maxima were spuriously produced in the likelihood test. The principal sources of error in the M/L_V estimates are (i) shot noise - we are inherently limited by the finite number of sources sampled within a few tidal radii of each lensing cluster galaxy, (ii) the spread in the intrinsic ellipticity distribution of the source population, (iii) the unknown source redshifts and (iv) observational errors arising from uncertainities in the measurement of ellipticities from the images for the faintest objects.

In their simulation NK (Section 4) showed that the strength of the signal and hence the significance of detection increases with increasing the mass-to-light ratio of the cluster galaxies as well as increasing the

total number of background galaxies. NK demonstrated (Section 4.3) that a cluster/background number ratio r of 0.02 would ensure a 3-σ detection for $\Upsilon \gtrsim 4$ for a cluster at z=0.175 and that the detection significance improved with $\sqrt{N_{bg}}$ as expected. However, these simulations, whilst realistic to the extent of incorporating the statistical properties of foreground and background galaxies according to various simple models, did not incorporate uncertainties arising from shot noise, possible uncertainties in estimates of the redshift distribution of background galaxies and instrumental effects such as the sampling and point spread function characteristics of WFPC-2. The unknown redshift distribution of the background sources will affect the retrieval of the signal in a systematic way. For instance, the total mass estimate for the cluster galaxies for a given shear would be under-estimated if the mean redshift of the background population was increased.

In the context of the HST data for AC114, we have therefore revisited these simulations. For the actual cluster/background ratio adopted in the observational analysis of AC114 ($r \sim 0.05$ - since the bulk of the signal arises predominantly from the brighter half of the perturbers), running NK's simulations we find that noise-free simulations would yield a 3-σ detection for $\Upsilon = 15$. In practice, the maximum likelihood contours in Fig. 3 yield a confidence level of approximately 1.7-σ illustrating the possible degradation introduced by noise.

We have also separated our sample of perturbers on the basis of their luminosity (bright/faint) and find that the majority of the power in our tests is, unsurprisingly, coming from the more luminous half of the sample, the mix of E vs S0 in the two samples is bright (36:40) and faint (34:44). Separating the sample using the radial distance from the cluster centre (inner/outer) showed no statistically significant differences between the two samples, again the mix of E vs S0 in the two samples is inner (32:37) and outer (49:37). The absence of any measurable radial variation in the properties of the cluster galaxy halos in our sample is not surprising given the limited sample size and area coverage. On combining comparable data sets for each of 10 clusters observed with the forthcoming *HST ACS* (*Advanced Camera for Survey*), our techniques would provide 99.5% confidence measurement of the fiducial parameters opening the way for the extension of this analysis to study the radial variation of the mass-to-light ratio within clusters.

6. Discussion and Conclusions

In this paper, we have reported the first detection of the signature of extended dark halos around galaxies in the rich cluster AC114 at $z = 0.31$. From our analysis we find that a L^* spheroidal cluster galaxy has a total mass of $M \sim (4.9^{+3.1}_{-1.3}) \times 10^{11}\, M_\odot$, and a $M/L_V \sim 15^{+10}_{-4}(M/L)_\odot$. We find that the **total** mass of a fiducial L^* cluster spheroidal is primarily contained with ~ 15 kpc, with some indication that the

halos of the S0 population may be more truncated than those of the ellipticals.

For field galaxies, with greater uncertainty, galaxy-galaxy lensing has been used to place constraints on halo sizes and masses of field galaxies on larger scales (BBS & DT). Comparing our results with those from both these field studies, we find an apparent halo cut-off in the cluster which is not seen in the field, $r_t \sim 15$ kpc in AC114 versus $r_t \gtrsim 200$ kpc (BBS) and $r_t \gtrsim 30$ kpc (DT) for the field. This would give some support to the hypothesis that the cluster galaxies have truncated mass profiles, as expected if they suffer substantial stripping of their dark matter halos during the formation of the cluster. Moreover, the evidence for smaller truncation radii in the S0 galaxies compared to the ellipticals would imply that they have suffered more stripping, possibly due to their less bulge-dominated (compact) mass distributions. These differences in the truncation radii found by the various studies lead to differences in the total masses inferred inside large apertures (larger than the truncation radii of some of the samples). We caution, however, that differences in the sample selection, observing conditions and methodologies for these studies make any accurate comparison complex. A similar *HST*-based survey of weak lensing by elliptical galaxies in the field (Ebbels et al. 1998) should provide the optimal field sample for detailed comparison with our results. The prospects for comparing the variation of the mass-to-light ratio for galaxies as a function of environment are promising.

Comparing the total mass in cluster galaxies within 250 kpc of the center (down to the magnitude limit of our selection criterion) to the total mass of the cluster, we estimate that approximately 11% of the mass of the cluster is bound to individual cluster galaxies. The fraction of the total cluster mass that is associated with individual galaxies has important consequences for the rate of galaxy interactions and hence the evolution of the cluster on the whole. The tidal field of the cluster potential well is strong enough to truncate the dark matter halo of a galaxy whose orbit penetrates the cluster core. In the context of this truncation picture, the tidally limited radius ($r_{\rm tidal}$) and mass of a cluster galaxy whose orbital pericenter is close to the cluster core radius can be estimated from (Merritt 1988):

$$r_{\rm tidal} \approx 30 \, (\frac{\sigma_{0*}}{240\,{\rm km\,s^{-1}}}) \, (\frac{\rho_0}{0.04\,M_\odot\,{\rm pc^{-3}}})^{-\frac{1}{2}} \ {\rm kpc}, \tag{11}$$

$$M \approx 1.4 \times 10^{12} \, (\frac{\sigma_{0*}}{240\,{\rm km\,s^{-1}}})^3 \, (\frac{\rho_0}{0.04\,M_\odot\,{\rm pc^{-3}}})^{-\frac{1}{2}} \, M_\odot \tag{12}$$

where ρ_0 is the central density of the cluster. Using the estimate of ρ_0 for AC114 from the strong lensing model ($\rho_0 = 0.0375\ M_\odot\, pc^{-3}$ and σ_0 from the maximum-likelihood analysis, we obtain $r_{\rm tidal} \sim 25$ kpc and an estimate of the mass enclosed within $r_{\rm tidal}$, $M \sim 9.0 \times 10^{11}\, M_\odot$; which compares well with the values obtained from the maximum likelihood analysis ($r_{\rm t} \sim 17$ kpc and $M \sim (4.9^{+3.1}_{-1.3}) \times 10^{11}\, M_\odot$). Dark halos of the scale of $\sim$ 15–30 kpc indicate a high probability of galaxy–galaxy collisions over a Hubble time within

a rich cluster. However, since the internal velocity dispersions of these cluster galaxies ($\sim$ 150–250 km s^{-1}) are much smaller than their orbital velocities, these interactions are unlikely to lead to mergers, suggesting that the encounters of the kind simulated by Moore et al. (1996) are the most frequent and likely.

These first results on the properties of galaxy halos within clusters from lensing are very encouraging. We are therefore extending our analysis using both observations of galaxies in the central regions of rich clusters at $z = 0.17$–0.56 (Natarajan, Kneib & Smail 1998) and across a range of environments within a number of clusters at $z \sim 0.3$. These two samples will provide insights into the role of changes in halo properties in the evolution of both cluster spheroids (Ellis et al. 1997) and disk galaxies (Couch et al. 1997), as well as the variation of these effects with local environment. The hope of future expansion of this technique appears good with the proposed installation of the the *ACS* in the next *HST* Servicing Mission, which will be able to cover a wider field providing the ideal data-sets for such studies. Similarly, progress is expected in the techniques and formalism used to constrain the mass distribution on different scales, taking full account of the noise in the ellipticity measurements. Therefore, the prospects for understanding the evolution of galaxy halos from field galaxies to cluster cores and hence the radial variation of the mass-to-light ratio are promising.

Acknowledgements

We acknowledge useful discussions during various stages of this work with Neta Bahcall, Tereasa Brainerd, Tim Ebbels, Marijn Franx, Josh Frieman, Bernard Geiger, Nick Kaiser, Chris Kochanek, Martin Rees, Peter Schneider and Simon White. JPK acknowledges support from the CNRS and IRS acknowledges funding from the Particle Physics and Astronomy Research Council.

REFERENCES

Bertin E. & Arnouts, S., 1996, A&A Supp., 117, 393.

Brainerd, T.G., Blandford, R.D. & Smail, I., 1996, ApJ, 466, 623 (BBS).

Connolly, A. J., Szalay, A. S., Dickinson, M. E., Subbarao, M. & Brunner, R., 1997, submitted.

Couch, W., Barger, A.J., Smail, I., Ellis, R.S. & Sharples, R.M., 1997, ApJ, submitted.

Cowie, L.L., Songaila, A., Hu, E.M. & Cohen, J.G., 1996, AJ, 112, 839.

Dell'Antonio, I. P., & Tyson, A. J., 1996, ApJ Lett., 473, 17 (DT).

Ebbels, T., et al, 1998 in prep.

Ellis, R. S., Smail, I., Dressler, A., Couch, W.J., Oemler, A. Jr, Butcher, H. & Sharples, R.M., 1997, ApJ, 483, 582.

Ellis, R.S., Ann Rev. 37, in press.

Geiger, B., & Schneider, P., 1997, preprint, astro-ph/9707044.

Holtzman, J.A., Burrows, C.J., Casterno, S., Hester, J.J., Trauger, J.T., Watson, A.M. & Worthey, G., 1995, PASP, 107, 1065.

Jorgensen, I., Franx, M. & Kjaergaard, P., 1996, MNRAS, 280, 167.

Kaiser, N. & Squires, G., 1993, ApJ, 404, 441.

Kaiser, N., 1995, ApJL, 439, 1.

Kassiola, A. & Kovner, I., 1993, ApJ, 417, 450.

Kassiola, A., Kovner, I. & Fort, B., 1993, ApJ, 400, 41.

Kneib, J-P., Ellis, R.S., Smail, I., Couch, W. & Sharples, R.M., 1996, ApJ, 471, 643.

Kneib, J.P., Pelló, R., Mellier, Y., Soucail, G., Fort, B., Ellis, R.S., Aragón-Salamanca, A., Smail, I., Miralda-Escudé, J., 1997, in prep.

Lanzetta, K., Yahil, A. & Fernandez-Soto, A., 1996, preprint, astro-ph/9606171.

Mellier, Y., et al 1997, Proceedings of the 37th Herstmonceux Conference, *HST and the high redshift Universe*, Cambridge.

Merritt, D., 1988, in ASP Conf. Series, *The Minnesota Lectures on Clusters of Galaxies and Large-scale Structure*, ed. Dickey, J., 175.

Metcalfe, N., Shanks, T., Campos, A. & Garner, J.P., 1996, Nature, 383, 236.

Mobasher, B., Rowan-Robinson, M., Georgakakis, A. & Eaton, N., 1996, MNRAS, 282, 7.

Moore, B., Katz, N., Lake, G., Dressler, A. & Oemler, A., 1996, Nature, 379, 613.

Natarajan, P. & Kneib, J-P., 1995, IAU Symp. 173, *Gravitational Lensing*, eds. Kochanek, C. & Hewitt J. (Springer).

Natarajan, P. & Kneib, J-P., 1997, MNRAS, 287, 833 (NK).

Natarajan, P., Kneib, J-P., & Smail, I., 1998, in prep.

Rix, H-W., de Zeeuw, T., Carollo, M., Cretton, N. & van der Marel, R., 1997, preprint, astro-ph/9702126.

Sackett, P., 1995, IAU Symp. 173, *Gravitational Lensing*, eds. Kochanek, C. & Hewitt J. (Springer).

Schneider, P. 1995, A&A, 302, 639.

Schneider, P. & Rix, H-W., 1997, ApJ, 474, 25.

Seitz, C. & Schneider, P., 1995, A&A, 297, 287.

Smail, I., Couch, W.J., Ellis, R.S. & Sharples, R.M., 1995a, ApJ, 440, 501.

Smail, I., Ellis, R.S., Fitchett, M.J. & Edge, A.C., 1995b, MNRAS, 273, 277.

Squires, G., Kaiser, N., Fahlman, G., Babul, A. & Woods, D., 1996, ApJ, 469, 73.

Zaritsky, D., Smith, R., Frenk, C.S. & White, S.D.M., 1993, ApJ, 405, 464.

Fig. 1.— The central regions of our *WFPC2* image of AC114. The area displayed is roughly 560×560 kpc in extent. We identify the various multiply-imaged features in the center of the cluster (c.f. Fig. 2 and §2). We also overplot the iso-density contours of our best fitting mass model for the cluster constrained by the geometry and redshifts of these features. The details of the model mass distribution are given in Table 1. The overplotted shear field corresponds to the model predictions for sources placed at $z = 1$.

Fig. 2.— A mosaic of the brighter multiply-imaged sources seen in the central region of AC114 is presented here. Starting with S1/S2 (top), these represents two images of a $z = 1.86$ galaxy, identified and spectroscopically confirmed by Smail et al. (1995a). However, they were unable to identify the counter-image S3 in their search of multi-colour ground-based images due to its proximity to a bright cluster elliptical. We show all three images of this remarkable object with a compact core and blue hook-shaped extension, which illustrates the striking symmetry shown by the various images. Next we present five images of a clumpy background source: A1–5, A4/A5 representing two images of the source merging across the radial critical line. Our detailed mass model for the cluster, normalised using the observed position of the critical line for source 'S' at $z = 1.86$, indicates that the source 'A' lies at $z = 1.67 \pm 0.15$ and provides a probable core radius for the cluster mass of $r_c \sim 50$ kpc. For the B images we predict $z = 1.17 \pm 0.10$. We note that the image B3/B4 corresponds to two merging images of the source, and its apparent higher surface brightness arises because of the unresolved nature of the source at the resolution of *WFPC2*. Finally, we come to the striking three image system, C1/C2/C3, with an estimated source redshift of $z = 2.1 \pm 0.3$. This partial-ring galaxy shows considerable internal structure on scales corresponding to ~ 200 pc at the source. Additionally, we find another candidate multiple image system (5 images) D1–D5 with predicted redshift $z = 1.18 \pm 0.10$. The source of images B and D have similar redshift and may have physical links. In each case the tick marks represent 1 arcsec.

Fig. 3.— Panel [a]: Maximum-likelihood retrieval of the fiducial parameters for cluster galaxies in AC114: the likelihood peaks at $r_t^* \sim 20$ kpc and $\sigma_0^* \sim 190$ km s^{-1} (marked by the intersecting dotted lines); and the inner 3 contour levels correspond respectively to 60%, 80% and 90% confidence limits The galaxy models used in this case correspond to constant mass-to-light ratio (i.e. $\alpha = 0.5$ was assumed in the scaling relations) which are the overplotted solid curves for $M/L_V = 10$, 17 & 23 (increasing from bottom to top). The secondary peak at $r_t \sim 50$ kpc is clearly insignificant (since the relevant contour demarcates only a 60% c. l. region), however if that higher value of r_t is to be taken seriously then it implies a mass that is larger by a factor of 2; Panel [b]: The fiducial parameters for the case when the the mass-to-light ratio scales with luminosity, i.e. $\alpha = 0.8$ in the assumed scaling relations. The recovered parameters with the maximum-likelihood in this case are: $r_t^* \sim 20$ kpc and $\sigma_0^* \sim 210$ km s^{-1} (marked by the intersecting dotted lines); and the inner 3 contour levels correspond respectively to 60%, 80% and 90% confidence limits and once again the overplotted solid curves correspond to the loci of constant $M/L_V = 13$, 23 & 27 (increasing from bottom to top) for a L^* galaxy; Panel [c]: Parameters recovered for the sub-samples: the cluster galaxies were split into 2 primary morphological classes the E's and the S0's. Combined optimization for their respective fiducial velocity dispersions yields: $\sigma_0^*(E) \sim 190$ km s^{-1} and $\sigma_0^*(S0) \sim 120$ km s^{-1}. The inner 3 contours correspond to 60%, 80% and 90% confidence limits. While the secondary peak seen is probably induced by the noise, the contours imply that at the 90% c.l. level the masses (or equivalently the truncation radii) of the Es and S0s are indistinguishable.

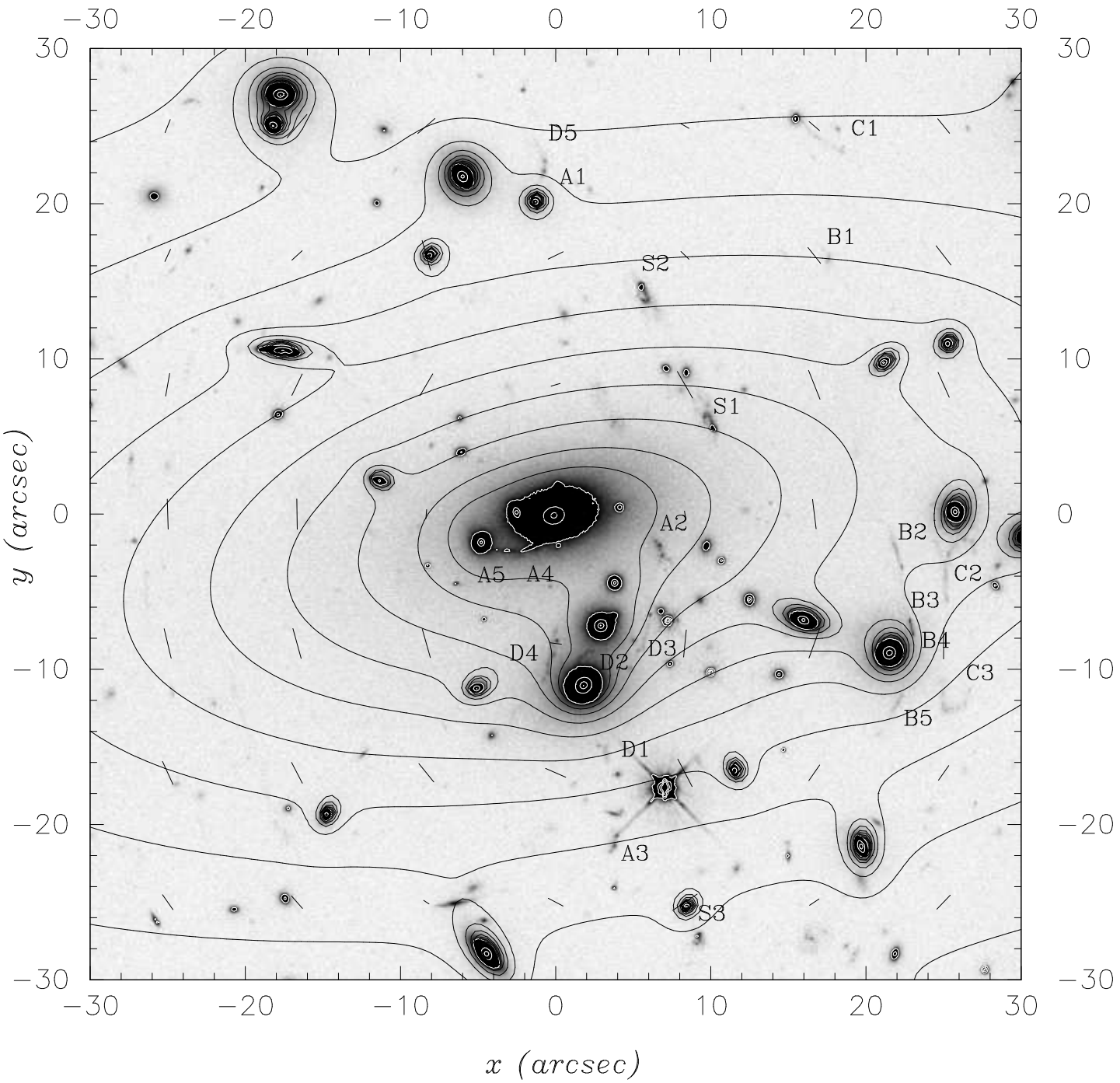
−30
−20
−10
0
10
20
30
y (arcsec)
x (arcsec)
D5
C1
A1
B1
S2
S1
A2
B2
C2
A5
A4
B3
D4
D2
D3
B4
C3
B5
D1
A3
S3

Table 1. Details of Mass Model for AC114

Cluster-Size Component	x_c (arcsec)	y_c (arcsec)	a/b	θ deg ree	r_c (kpc)	σ (km/s)	r_t (kpc)
Central potential	0.0 ± 0.5	0.0 ± 0.5	2.1 ± 0.1	$12. \pm 2.$	$105. \pm 5$	1080 ± 10	$650^{\pm}50$
Clump # 1	-160.0 ± 10	-15.0 ± 10	1.25 ± 0.1	-30 ± 10	150(fixed)	650 ± 50	400(fixed)
Clump # 2	75.0 ± 10	$-50. \pm 10$	1.2 ± 0.1	10 ± 10	100(fixed)	400 ± 50	400(fixed)

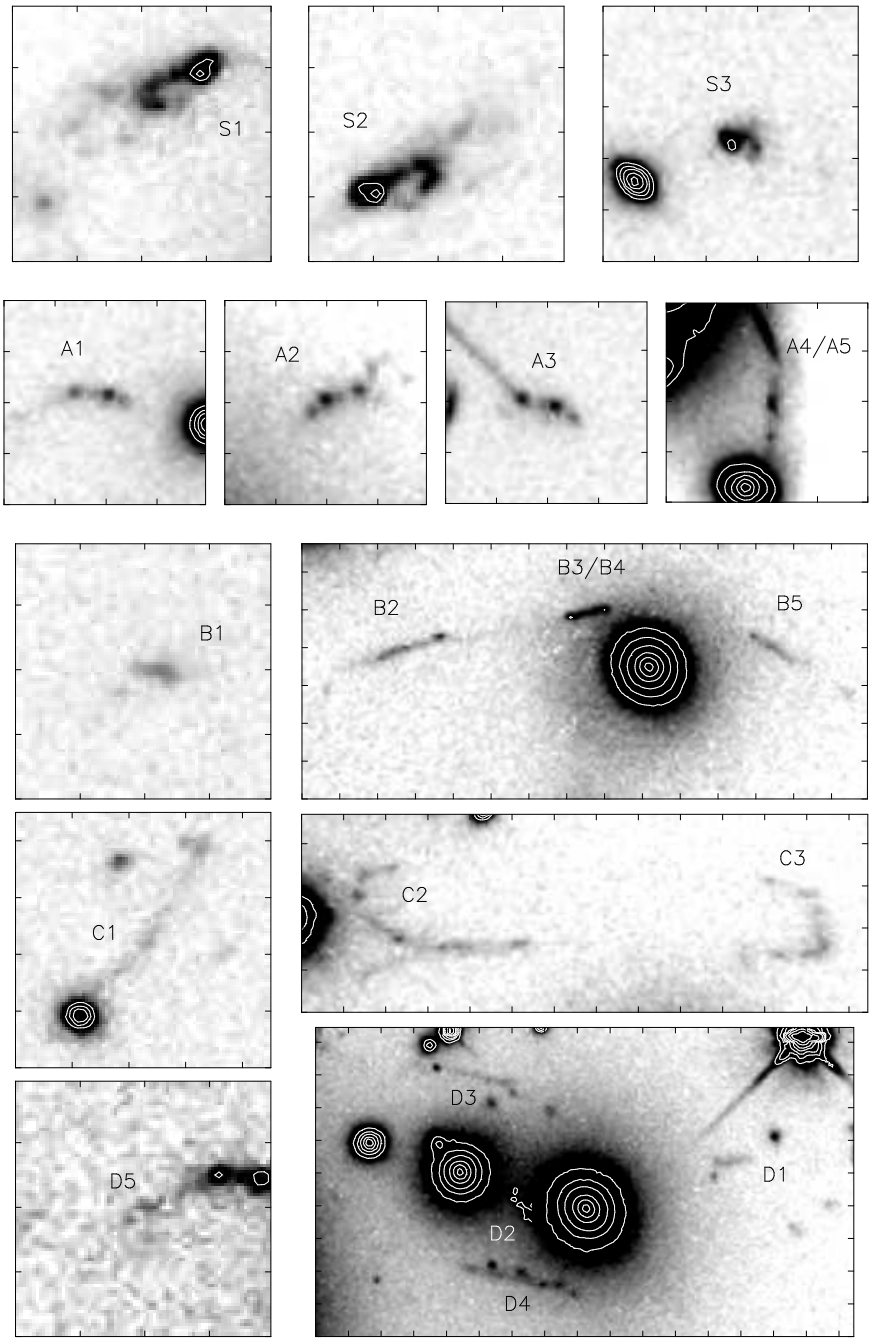
S1
S2
S3
A1
A2
A3
A4/A5
B1
B3/B4
B2
B5
C1
C2
C3
D5
D3
D1
D2
D4

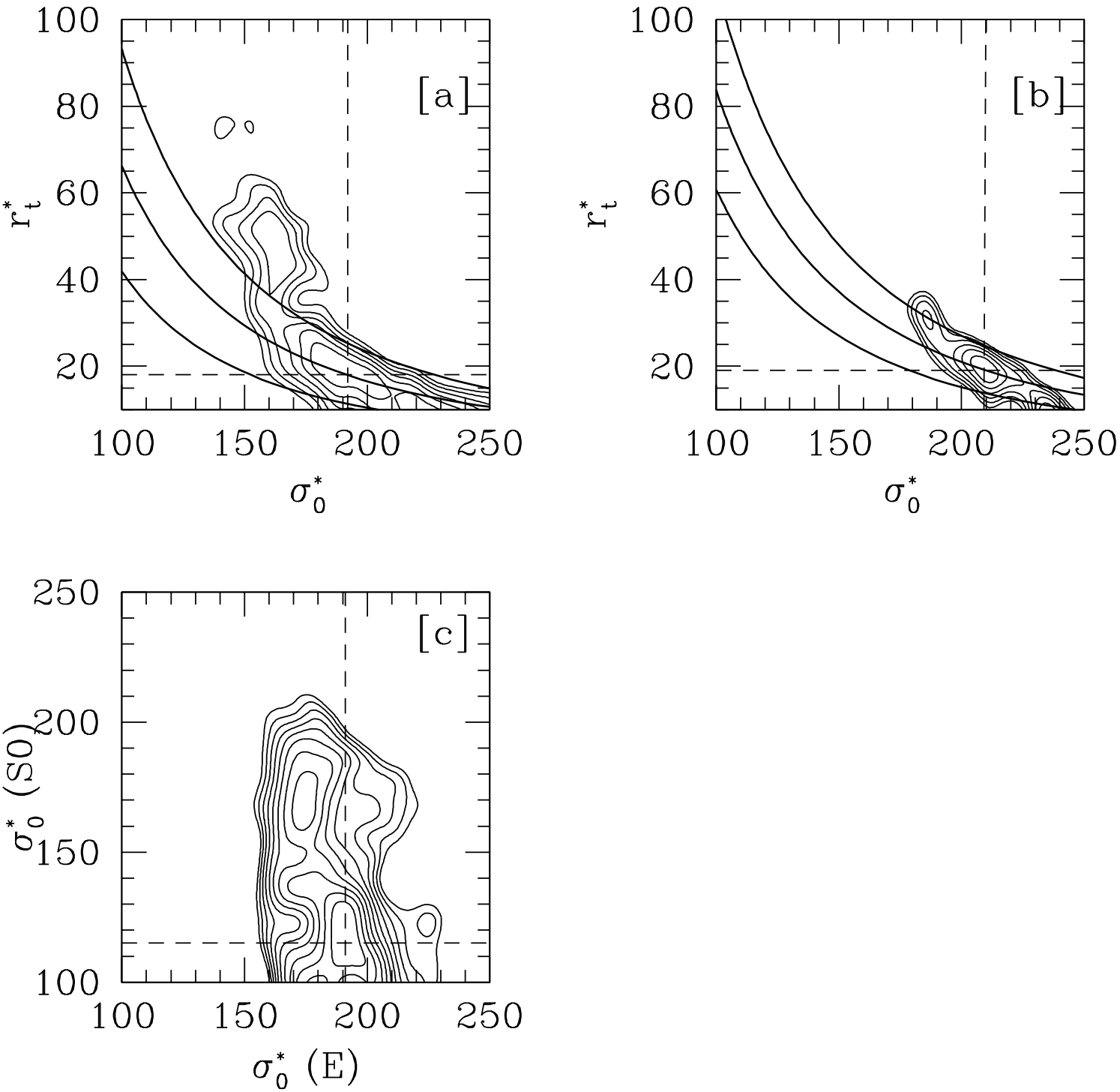
[a]
[b]
[c]
100
80
60
40
20
r_t^*
100
150
200
250
σ_0^*
σ_0^* (S0)
σ_0^* (E)